Outer-shell photodetachment of the metastable Be⁻ $1s^2 2s 2p^2$ $^4P^e$ state

José Luis Sanz-Vicario

GFAM, Instituto de Física, Universidad de Antioquia, Calle 67 No. 53-108, AA 1226, Medellín, Colombia

Eva Lindroth

Atomic Physics, Stockholms Centrum För Fysik, Astronomi och Bioteknik (SCFAB), Stockholm University, S-106 91 Stockholm, Sweden

We report calculated photodetachment cross sections from the metastable Be⁻ $1s^2 2s 2p^2$ $^4P^e$ state in the photon energy range 0–10 eV. Outer-shell photodetachment takes place in this energy range, which includes the double-ionization threshold Be⁺($^2S^e$) at ~7 eV as well as doubly excited thresholds of the residual atom up to the Be($1s^2 2p 4f$) threshold at ~10 eV. Therefore, triply excited states of Be⁻ are reached within the selected photon energy. We have implemented the complex scaled configuration interaction method along with a model potential for the $1s^2$ core to uncover the first series of Be⁻ $^4L^o$ resonant states. In this work, four $^4P^o$, seven $^4D^o$, and two $^4S^o$ resonances are reported and we compare our cross section with other previous theoretical calculations, that reported none or, at most, two resonances.

PACS number(s): 32.80.Gc, 31.25.Jf, 31.15.Ar

I. INTRODUCTION

In the last decade, negative atomic ions have received substantial attention by the atomic physics community [1]. Nowadays these systems have become the subjects of benchmark studies for different theoretical computational methods dealing with highly correlated systems. Strongly correlated excited states in negative ions should show up as specific features in photodetachment spectra, revealing details of their structure and dynamics. Three-electron atomic systems are at the edge of complete *full ab initio* treatments with today's computational facilities and their resonant states and photodetachment spectra are calculated with uncertainties of a few meV. In this work, we are interested in the outer-shell photodetachment of Be⁻ and we are then required to describe as accurately as possible the correlated motion of the three-valence electrons. Configuration interaction (CI) codes may be extended to treat many-electron systems that could be divided in an inert core plus active electrons. The beryllium negative ion may be treated as an effective CI three electron problem by using an appropriate model potential to describe the effect of the inner $1s^2$ core. The use of analytical model potentials in atomic structure is reported with profusion in the literature [2,3].

Long-lived states of Be⁻ ion were observed almost forty years ago in experiments [4], but it was Bae and Peterson [5] who first clearly identified the Be⁻ $(1s^2 2s 2p^2$ $^4P^e)$ as a metastable state and predicted its decay rate. The ground state of Be $(1s^2 2s^2$ $^1S)$ has a closed-shell configuration and it is stable enough so that adding an extra ns or np electron does not create a bound state, but a Be⁻ $(1s^2 2s^2 2p$ $^2P^o)$ shape resonance. It is instead the first excited triplet state of Be $(1s^2 2s 2p$ $^3P)$ that supports an extra $2p$ electron to produce the lowest discrete state of Be⁻ $(1s^2 2s 2p^2$ $^4P^e)$. Although electron correlation in configurations with spin unpaired electrons generally is less important, in this case it becomes crucial. Actually, Hartree-Fock calculations place the Be⁻ $(1s^2 2s 2p^2$ $^4P^e)$ state above the parent state Be $(1s^2 2s 2p$ $^3P)$ [6]. Therefore, a good account of electron correlation is of the utmost importance. With the reasonable assumption that the $1s^2$ core is almost inert, the stability should be provided by the L-shell electron correlation, being greater for the Be⁻ $2s 2p^2$ configuration than for Be $2s 2p$. This assumption tells us that we can restrict ourselves to consider only the strong interaction for the three outer-shell electrons, taking the electron-core interaction into account through a suitable model potential. A similar procedure, but within an R-matrix approach, was employed by Kim and Greene [7]. In this work, we make use of an extension of the complex scaled configuration interaction (CSCI) method, successfully applied previously in our laboratory to pure three-electron systems, such as He⁻ [8,9]. Complex scaling methods have already been applied to study the Be⁻ $1s^2 2s^2 \epsilon p$ shape resonance [10–12] with a multiconfigurational self-consistent-field method. Anyway, albeit Be⁻ may be thought of as a simple system, it turns out to be quite an unexplored ion in its resonant structure.

Three metastable states form the known discrete spectrum of the beryllium negative ion [13] (see Fig. 1); Be⁻ $1s^2 2s 2p^2$ $^4P^e$, mentioned above, Be⁻ $1s^2 2p^3$ $^4S^o$, below the Be $1s^2 2p^2$ ^3P, and Be⁻ $1s 2s 2p^3$ $^6S^o$, below the Be $1s 2s 2p^2$ ^5P (outside the energy range shown in Fig. 1). The Be⁻ $^4S^o$ state can decay radiatively to the lowest-energy state $1s^2 2s 2p^2$ $^4P^e$.

The initial state in our photodetachment study is the metastable state Be⁻ $1s^2 2s 2p^2$ $^4P^e$, with an averaged experimental lifetime of $\tau \sim 45$ μs [14], long enough to be used in photodetachment experiments. Unfortunately, experiments involving beryllium species have almost disappeared from laboratories due to strict regulations to manipulate dangerous substances. Furthermore, photodetachment experiments on Be⁻ turned out to be a difficult task and they remain a challenge. As a matter of fact, only two photodetachment experiments on Be⁻ have been reported so far [5,15] and they show contradictory results. Therefore, the theoretical input is crucial to partially relieve this difficulty.

On the theoretical side, things have not been much better. To our knowledge, only four-cross-section calculations are
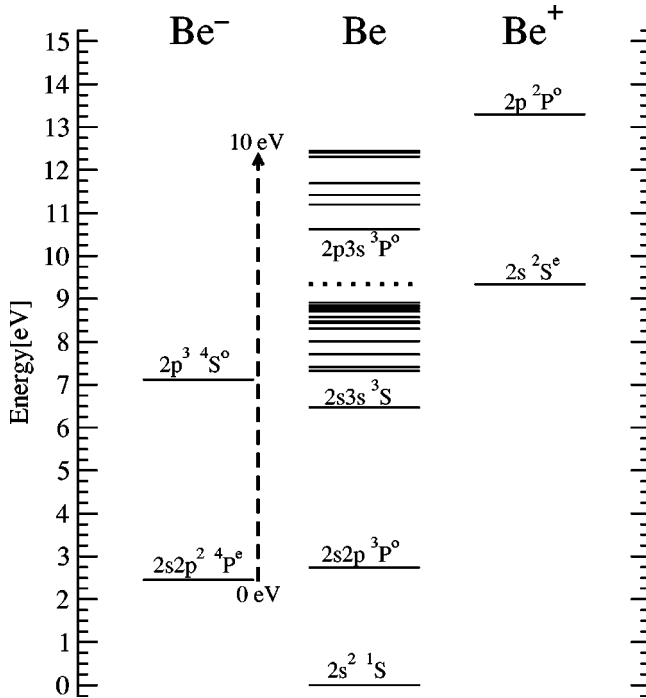
FIG. 1. Scheme of states of Be^-, Be, and Be^+ relevant to our photodetachment study. The photon energy scale is reset to zero at the first metastable state of Be^- and the thick dashed arrow covers the full range of photon energy (0–10 eV) in this work.

available today in the literature. Those of Sinanis et al. [16], with a state-specific configuration interaction method, and Ramsbottom and Bell [17], with a R-matrix method, do not show any resonant structure. The calculation by Xi and Froese Fischer [18], using a Galerkin inverse-iterative method, predicts one sharp $^4P^o$ resonance and the latest calculation by Zeng et al. [19], also with a modified R-matrix, shows two $^4P^o$ resonances. In this work, we calculate the photodetachment cross section through a completely different method with a high level of sophistication. We obtain a coarse agreement with the previous results aforementioned. In addition, we locate four $^4P^o$, seven $^4D^o$, and two $^4S^o$ resonances and their parameters (position and widths) are given.

II. METHOD

Depending on the type of system, different atomic model potentials have been proposed to describe the inert core, with different level of sophistication. For the simple case of the $1s^2$ core, polarization effects are not particularly important and the potential due to the two $1s$ electrons may have the form

$$V^{model}(r) = \frac{2}{r} - \frac{2}{r}(1+\alpha r)e^{-2\alpha r}, \qquad (1)$$

where α is a parameter conveniently adjusted. This model potential has been previously used, for instance, to calculate bound states of three- and four- electron atoms and, more specifically, bound and resonant states of Be-like ions [20].

This model potential is justified because it reproduces the form of the Hartree-Fock potential $2V^{direct} - V^{exchange}$ for an electron in the presence of a $1s^2$ core. Alternative model potentials depending on three parameters, both l-dependent and l-independent, has been proposed by Aymar et al. [21] for the alkaline earths. These one-particle potentials are built empirically to provide accurate ionization energies of $1s^2nl$ Be^+ states. The parameter α is adjusted until the eigenvalues ϵ_{nl} obtained from the one-electron reduced radial equation,

$$\left[-\frac{1}{2}\frac{\partial^2}{\partial r^2} + \frac{l(l+1)}{2r^2} - \frac{Z}{r} + V^{model}(r) \right] P_{nl}(r) = \epsilon_{nl}P_{nl}(r), \qquad (2)$$

agree with the tabulated experimental energies. In this work, we make use of the uniform complex scaling where the radial electron coordinate is complex rotated ($r \rightarrow re^{i\theta}$). We have adjusted the optimal parameter α when the rotation angle θ is zero and then complex scaling is applied normally. While the kinetic and Coulomb terms are easily factorized, the model potential term is nonlinear. The application of complex scaling over nonlinear analytical potential showing resonances has been tested before with illustrative potentials $V(r) = Ar^2e^{-r}$ and $V(r) = Ae^{-a(r-r_0)} - Be^{-br^2}$ [22]. Because of the complex rotation, the potential splits in real and imaginary part. The imaginary part acts to comply with the L^2 integrability of the rotated continuum wave function. When the potential contains exponential terms the complex rotation shows an oscillatory behavior, both in the real and imaginary part, that is more prominent as the rotation angle increases. The global distortion due to the complex scaling affect the bound and continuum energies of the Be^+ differently. Theoretically, bound states remain unchanged by the rotation, although in practical computations they change slightly, separating from the real abscissa. These slight changes in bound states seem to be more sensitive in the one-electron eigenvalues given by Eq. (2) than in pure hydrogenic systems. We thus avoid large rotation angles (we use $\theta = 8° - 16°$ in this work), to keep our Be^+ bound states with a minimal distortion over the real axis but just enough to uncover the Be^- resonances.

The alkaline-earth negative ions may be described by the three-electron Hamiltonian

$$H = \sum_i h_i^{model} + \sum_{i<j} \frac{1}{r_{ij}}, \qquad (3)$$

where the sums involve only the three outer-shell electrons and the expression for the model Hamiltonian h^{model} is given by Eq. (2).

The one-electron radial function $P_{nl}(r)$ is expanded in terms of N B-splines (a set of piecewise polynomials) confined in a box of length $[0,r_{max}]$, where r_{max} is the box size. The model Hamiltonian is projected onto the B-spline basis set and the complex symmetric eigenvalue problem is solved by standard routines. The complex eigenfunctions of Eq. (2) are then used to build three-electron configurations adapted to the total $L,S,$ and parity π. The matrix elements of the

effective three-electron Hamiltonian of Eq. (3) are evaluated and the much bigger associated generalized eigenvalue problem is solved again.

Once the three-electron eigenfunctions are obtained, the photodetachment cross section as a function of the photon energy is calculated with the expression [23]

$$\sigma(\omega) = \frac{1}{2L_0+1} \frac{e^2}{4\pi\epsilon_0} \frac{4\pi}{3} \frac{\omega}{c} \text{Im} \left(\sum_n^M \frac{\langle \Psi_0 | \widetilde{\mathbf{P}} | \Psi_n \rangle^2}{\widetilde{E}_n - E_0 - \hbar\omega} \right),$$
(4)

where Ψ_0 denotes the initial-state wave function with an energy E_0, Ψ_n corresponds to the final state of complex energy $\widetilde{E}_n$, let them be bound, resonant or continuum states and $\widetilde{\mathbf{P}} = \Sigma_{i,q} r_i e^{i\theta} \mathbf{C}_i^{(q)}$ is the rotated dipolar operator.

III. RESULTS AND DISCUSSION

The initial state here considered is Be$^-$ $1s^2 2s 2p^2$ $^4P^e$ and thus the final states are $^4P^o$, $^4D^o$, and $^4S^o$. Thus, the total photodetachment reaction reads as follows:

$$\text{Be}^-(1s^2 2s 2p^2\,^4P^e) + \hbar\omega \rightarrow \sum_{^4L^0} [\text{Be}(1s^2 nln'l')^3 L_1$$

$$+ \epsilon(n''l'')]^4 L^0,$$
(5)

where $\hbar\omega$ denotes the photon and ϵ corresponds to the energy of the detached photoelectron. In the photon energy range studied in this work, from 0 to 10 eV, the label nl in Eq. (5) represents $2s$ and $2p$ orbitals only, and $n'l'$ may reach up to $n'=6$ (the threshold Be $1s^2 2s 6p$ $^3P^o$ at ~ 6.5 eV) and to $n'=4$ (the threshold Be $1s^2 2p 4f$ $^3F^o$ at ~ 10 eV), respectively. Note that the double ionization threshold (i.e., Be$^+$ $^2S^e$) lies in this photon energy range at ~ 6.9 eV. Therefore, double-photodetachment channels should be rigorously included and in our CSCI method they are taken into account.

First, we solve the one-electron eigenvalue problem of Eq. (2). for the Be$^+(1s^2 nl)$ states with a basis set of 20 B splines of order $k=7$, a box length of 120 a.u., and l-dependent parameters α^l ($\alpha^0 = 2.3518664$, $\alpha^1 = 2.361045$, $\alpha^2 = 2.17110$, and $\alpha^3 = 1.580$), adjusted to provide the experimental lowest eigenvalue for each l symmetry. In Table I, we include our energies for the Be$^+$ $(1s^2 nl)$ states. To compare, we also report previous calculations [20] with the same model potential but with an almost complete Slater-type basis set and the experimental results from Ref. [24]. We also calculate *ab initio* Hartree-Fock orbital energies corrected by a polarization potential as done in Ref. [25]. This polarization correction added to the Hartree-Fock orbitals does not provide the required accuracy for the lowest nl orbitals ($2s$, $2p$), although it is improved as n increases. Other results to compare with can be found in Table II of Ref. [20]. We conclude that our results are very satisfactory, given the limited number of included B-splines. By using l-dependent model potentials, one may introduce complications due to the fact that all orbitals are not eigenfunctions of the same Hamiltonian operator. We have also

TABLE I. Energies (in atomic units) of $1s^2 nl$ states of Be$^+$ ion. The values are referred to the Be^{2+} $(1s^2)$ core.

nl	Model potential	Reference [20]	HF+pol	Expt. Reference [24]
$2s$	$-0.669\,246$	$-0.669\,248$	$-0.669\,703$	$-0.669\,246$
$3s$	$-0.267\,649$	$-0.267\,685$	$-0.267\,292$	$-0.267\,233$
$4s$	$-0.143\,354$	$-0.143\,381$	$-0.143\,169$	$-0.143\,153$
$5s$	$-0.089\,166$	$-0.089\,196$	$-0.089\,067$	$-0.089\,065$
$2p$	$-0.523\,768$	$-0.523\,718$	$-0.522\,950$	$-0.523\,768$
$3p$	$-0.229\,819$	$-0.229\,798$	$-0.229\,317$	$-0.229\,582$
$4p$	$-0.128\,259$	$-0.128\,255$	$-0.128\,021$	$-0.128\,134$
$5p$	$-0.081\,645$	$-0.081\,687$	$-0.081\,548$	$-0.081\,610$
$3d$	$-0.222\,478$	$-0.222\,404$	$-0.222\,468$	$-0.222\,478$
$4d$	$-0.125\,143$	$-0.125\,103$	$-0.125\,120$	$-0.125\,124$
$5d$	$-0.080\,068$	$-0.080\,018$	$-0.080\,064$	$-0.080\,067$

checked this point and we find that differences by using l-dependent or l-independent potentials in our three-electron CI calculation are negligible. Actually, the l-dependency of the model potential does not give much better improvement for the Be$^+$ energies in comparison with l-independent ones ($\alpha = \alpha^0$) because the main discrepancy between the model potential V^{model} and $2V^{direct} - V^{exchange}$ comes from the exchange part, and this term varies as a function of n and not l, as discussed in Ref. [20]. Additionally, core-polarization plus dielectronic polarization terms added to the model potential [26] could modify slightly the value. It has been pointed out that core-valence and core-core correlation must be included to obtain accuracies to within a few meV [27]. For cores such as Mg^{2+} and Ca^{2+}, these corrections are important, but for the simple Be^{2+} core, it has been shown that more complicate model potentials including polarization terms provide results that compare similarly with ours and with the experimental results. Li$^-$ that has an identical core and where accurate experiments are available has been successfully described by simple polarization potentials [25,28,29] which support the idea that something similar should be possible here. Furthermore, we decide to keep the model potential for Be$^{2+}(1s^2)$ as simple as possible (in order to complex rotate it) but, simultaneously, accurate enough.

For each three-electron L,S,π symmetry, we select three-electron $nln'l'n''l''$ type configurations built from s, p, d, and f orbitals. The three-electron basis set of configurations used in this work is listed in Table II. Within the space spanned by the selected configurations, the Be target states (all thresholds listed in Table III) must be appropriately represented. For instance, the Be $1s^2 2s n'p$ $^3P^o$ and Be $1s^2 2p n's$ $^3P^o$ thresholds plus ϵs or ϵd escaping electrons, are accounted for with spp-type configurations from the $^4P^e$ symmetry , ssp and spd from the $^4P^o$ symmetry, and spd from the $^4D^o$ symmetry. In most cases in our calculations, n' and n'' reach values up to 18 for the outermost electrons and then we expect to obtain a reasonable accuracy to reproduce thresholds in the whole photon energy range. We must

TABLE II. $ll'l''$−type and number N of configurations used to calculate resonances and photodetachment of Be$^-$ $^4P^e$. $ll'l''$-type configurations are indicated as $n_1,n_2,n_3ll'l''$ and N indicates the number of configurations for every $ll'l''$ type of configuration.

$^4P^e$	N	$^4P^o$	N	$^4D^o$	N	$^4S^o$	N
13,17,18spp	1836	12,17,18ssp	1980	17,12,18spd	3456	18,18,18ppp	1140
13,17,18sdd	1836	18,17,12spd	3468	17,18,12sdf	3456	18,18,18pdd	3078
13,17,18sff	1836	11,17,18sdf	3060	5,15,18ppp	1165	18,18,15pff	2565
3,17,18ppd	1674	1,12,17ppp	357	10,18,5ppf	1300	10,18,18ddf	2430
2,17,18pdf	1224	1,12,17ppf	187				
1,17,18ddd	475	1,12,17ddp	210				
Total	9323		9262		9377		9213

remark that in our method the Be threshold energies are obtained directly from the diagonalization of the Be$^-$ problem. In other approaches, such as R-matrix and Galerkin inverse-iterative methods, the Be target energies are calculated previously as accurately as possible and then the channels Be $+\epsilon(n''l'')$ are explicitly constructed. If not accurate enough, diagonal elements in the Hamiltonian matrix may be adjusted to reproduce the Be experimental energies [17].

The initial state Be$^-$ $1s^22s2p^2$ $^4P^e$ has been calculated with 9323 configurations and the energy we obtained is $E_0 = -0.921\,945\,69$ a.u. with respect to the Be^{2+} energy. This can be compared with the most accurate value of $-0.922\,311$ a.u., obtained from the difference between the total binding energy of Be$^-$ $1s^22s2p^2$ $^4P^e$, $-14.577\,877$

TABLE III. Thresholds of the Be$^-$ system. The experimental values are taken from NIST [30]. Energies are given in eV and relative to the Be$^-$ $(1s^22s2p^2$ $^4P)$ state.

State	Expt. (NIST)	This work	Reference [18]
1 Be($1s^22s2p$ $^3P^o$)	0.290 990	0.2876	0.2867
2 Be($1s^22s3s$ ^3S)	4.023 013	4.0112	3.9967
3 Be($1s^22s3p$ $^3P^o$)	4.869 419	4.8582	4.8442
4 Be($1s^22p^2$ ^3P)	4.967 164	5.1252	4.9953
5 Be($1s^22s3d$ ^3D)	5.259 481	5.2527	5.2409
6 Be($1s^22s4s$ ^3S)	5.563 580	5.5447	7.4850
7 Be($1s^22s4p$ $^3P^o$)	5.849 417	5.8063	8.1223
8 Be($1s^22s4d$ ^3D)	5.989 492	5.9552	8.0253
9 Be($1s^22s4f$ $^3F^o$)	6.026 608	6.0047	
10 Be($1s^22s5s$ ^3S)	6.121 974		
11 Be($1s^22s5p$ $^3P^o$)	6.252 803		
12 Be($1s^22s5d$ ^3D)	6.319 551		
13 Be($1s^22s5f$ $^3F^o$)	6.337 648		
14 Be($1s^22s6s$ ^3S)	6.388 580		
15 Be($1s^22s6p$ $^3P^o$)	6.459 264		
limit Be II ($^2S^e$)	6.888 500	6.633 95	
16 Be($1s^22p3s$ $^3P^o$)	8.173 652	8.1550	8.1913
17 Be($1s^22p3p$ ^3D)		8.7475	8.7425
18 Be($1s^22p3p$ ^3P)	8.974 455	8.9784	8.9840
19 Be($1s^22p3d$ $^3D^o$)	9.243 820	9.2421	9.4076
20 Be($1s^22p4p$ ^3P)	9.860 781	9.8394	
21 Be($1s^22p4d$ $^3D^o$)	9.962 285	9.9344	
22 Be($1s^22p4f$ $^3F^o$)	9.992 887		

a.u., from Ref. [31] and the total binding energy of the Be^{2+} ground state from Ref. [32], $-13.655\,566$ a.u. The electron affinity of Be $1s^22s2p$ ^3P, i.e., E(Be$^-$ $1s^22s2p^2$ $^4P^e$) $-E$(Be$1s^22s2p$ ^3P), can be estimated from our calculation if the Be $1s^22s2p$ ^3P threshold is obtained by extrapolating the lowest-energy continuum branch (Be $1s^22s2p$ ^3P plus an outgoing electron) to the real axis, i.e., to zero energy for the outgoing electron. We then obtain an affinity of 287.6 meV (1 a.u.$=27.209\,739\,7$ eV for Be) in rather good accordance with the most accurate theoretical values, 285 ±5 meV by Olsen $et\ al.$ [27], 289.1±1.0 by Hsu and Chung [31], and 286.7 meV by Xi and Froese Fischer [18]. The most recent experimental value is 290.99±0.10 meV by Kristensen $et\ al.$ [33]. The main error in our value comes from the approximate treatment of the $1s^2$- core correlation in the presence of the three outer electrons, as can be seen by comparison with Ref. [31].

Be($1s^22s4s$ ^3S), Be($1s^22s4p$ $^3P^o$), and Be($1s^22p3d$ $^3D^o$) thresholds reported by Xi and Froese Fischer [18] do not match the NIST data or ours (see Table III) and we presume there is a mistake in their tabulation. Our thresholds quoted in Table III are taken from the $^4P^o$ calculation, following the procedure aforementioned. Values from $^4D^o$ and $^4S^o$ symmetries are very similar within a ±1–5 meV error band on an average. In spite of our large size calculation, some Be thresholds are not obtained accurately, due to the $nl,n'l',n''l''$ asymmetries in the included configurations (i.e., not all electrons are allowed to reach the highest hydrogenic orbitals, due to limitations of our computational resources). For instance, the upper Be thresholds, corresponding to the Rydberg series that converges to Be$^+$ limit contain uncertainties, specifically when more than one channel is open, and we do not report those values in Table III. We also remark that the Be($1s^22p3p$ ^3D) threshold at ~8.74 eV (obtained also by Xi and Froese Fischer [18]) is not listed in the NIST database.

In Fig. 2, we plot the photodetachment cross section to the final $^4P^o$ states from 0 to 10 eV. Two major Feshbach resonances are revealed. The cross section by Ramsbottom and Bell [17] (they report from ~0.5 eV to ~4.3 eV) and Zeng $et\ al.$ [19] (from ~0.25 eV to ~6.7 eV) are also included. The cross section from Ref. [17] neither covers the region of the nonresonant peak after the $2s2p$ $^3P^o$ threshold nor does it displays the first resonance. Nonetheless, its background matchs ours perfectly. Fig. 4 in Ref. [18] shows the $^4P^o$
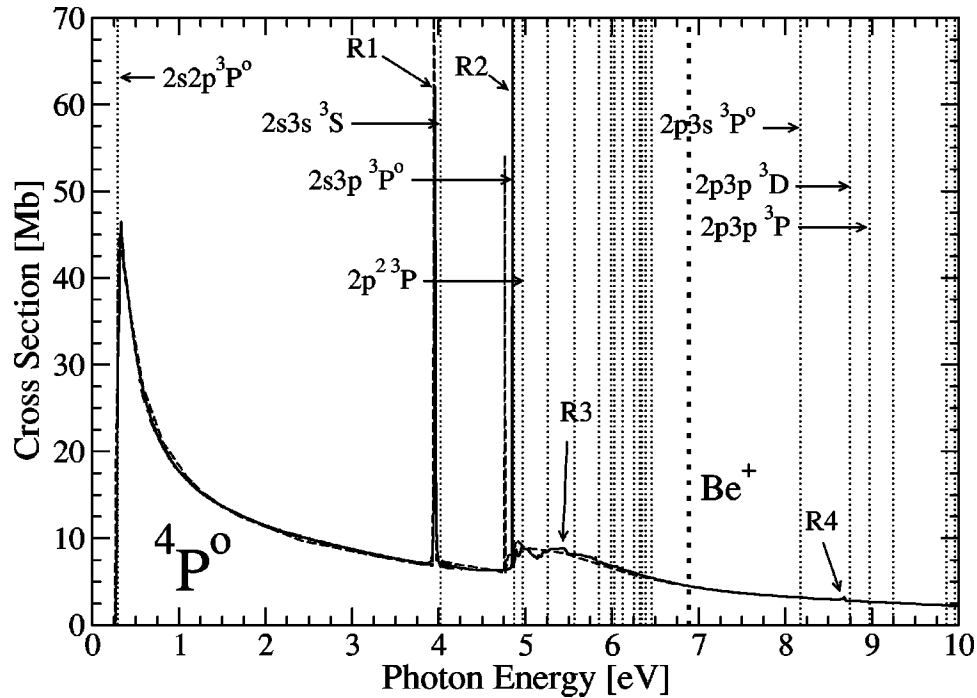
FIG. 2. Calculated photodetachment cross section to Be⁻ $^4P^o$ from the metastable Be⁻ $1s^22s2p^2$ $^4P^e$ state. Solid line, this work, dashed line, R-matrix by Zeng *et al.* [19], dash-dotted line, R-matrix by Ramsbottom and Bell [17] (it overlaps our background). The vertical dotted lines indicate Be thresholds $1s^2$ $nln'l'$ $^3L^\pi$ taken form the NIST database (the core $1s^2$ is omitted in the figures) quoted in Table III; the vertical thick dotted line indicates the position of the Be⁺ doubly ionization threshold. Resonance positions are labeled with Rn and the arrows point out to the maximum cross section of the CSCI calculation, except R2 (our peak reaches 116 Mb).

cross section via the Be($1s^22s2p$ $^3P^o)ks+kd$ channels, providing most of the contribution and it reflects a similar background from 0.5 eV and, the most important, displays the first resonance R1. That same Fig. 4 shows the contribution from other excited channels after the Be($1s^22s3p$ $^3P^o$) threshold, producing a raising shoulder. These excited channels are implicitly included both in Ref. [19] and in our calculation. The R-matrix calculation by Ref. [19] matches our cross section of the first nonresonant peak after Be ($1s^22s2p$ $^3P^o$) threshold, but the parameters of the two noticeable resonances R1 and R2 differ slightly in position and notably in the maximum cross section. Our resonance R1 is located at $E_{R1}=3.9579$ eV and we obtain a width $\Gamma_{R1}=11.21$ meV, in good agreement with 3.944 63 eV and 11.16 meV, respectively, from Xi and Froese Fischer [18] and 3.9454 eV from Ref. [19]. The difference in position should be attributed to the different calculated value of the Be($1s^22s3s$ ^3S) threshold, 4.0112 eV in our work and 3.9967 eV in Ref. [18]. The distance from the resonance position to the threshold differs only by 1 meV. Our resonance $^4P^o$ R1 reaches ~62 Mb, slightly higher than in Ref. [18] (~54). Reference [19] does not display the maximum cross section (but it is >60 Mb). Our resonance R2 is located at $E_{R2}=4.8491$ eV and its width $\Gamma_{R2}=0.632$ meV, which makes the resonance extremely sharp and therefore difficult to catch with coarse photon energy grids (we use here 30 000 points). This second resonance R2 has been reported previously only by Ref. [19], with a position of 4.7617 eV but no width. The maximum cross section differs strongly; ours is 116 Mb but it is given to around 55 Mb in

Ref. [19]. Again the difference in the position of resonance R2 may come from the calculated Be ($1s^22s3p$ $^3P^o$) threshold. This Feshbach resonance is located very close to that threshold (compare our Fig. 2 with 1 in Ref. [19]). Therefore, we conclude that a more accurate position should be near the NIST threshold position 4.8694 eV and we believe that our data is more reliable. We have not a clear answer about the discrepancy in the maxima. Both $^4P^o$ R1 and R2 resonances do not show any strong interaction with the underlying continuum. In fact, by performing a Fano-shape parametrization of the isolated resonance [25], we get a maximum of 55.6 Mb for R1 and 113 Mb for R2, respectively.

From the Be($1s^22s3p$ $^3P^o$) threshold at ~4.87 eV, the new opening of channels are well accounted for by Zeng *et al.*, Xi and Fischer in their Figure 4 and in our results, the last two showing a similar oscillatory pattern. Furthermore, we found two additional but small $^4P^o$ resonances; R3, a broad shape resonance located at $E_{R3}=5.4673$ eV and width $\Gamma=57.7$ meV and R4, $E_{R4}=8.6840$ eV and $\Gamma=28.8$ meV. R4 resonance lies above the double-ionization threshold Be⁺ and it corresponds to a resonant triply excited state of Be⁻. Table IV contains a summary of our resonance parameters. Also Fig. 3 displays the position of the $^4P^o$ resonances (S-matrix poles) in the complex plane.

In Fig. 4, we show the cross section to the final $^4D^o$ symmetry. Since we are more interested in the resonant structures close to the Be ^3D and ^3P thresholds, we stress the importance of appropriately well-balanced spd, sdf, and ppp configurations. In this symmetry, the number of configurations generated from s, p, d, and f orbitals increases

TABLE IV. Be$^-$ $^4P^o$, $^4D^o$, and $^4S^o$ resonance parameters in the photon energy region 0–10 eV. E_r is the binding energy relative to the ground state of Be^{2+}, while the position is relative to the Be$^-$ ($1s^2 2s2p^2$ ^4P) state.

	Resonance	E_r	$-\Gamma/2$	Position (eV)	Width (meV)	q (Fano parameter)
$^4P^o$	R1	$-0.776\,4849$	-2.060×10^{-4}	3.9579	11.2	-107
	R2	$-0.743\,7331$	-1.162×10^{-5}	4.8491	0.632	-37.4
	R3	$-0.721\,0145$	-1.060×10^{-3}	5.4673	57.7	-1.43
	R4	$-0.602\,7917$	-5.291×10^{-4}	8.6840	28.8	-2.74
$^4D^o$	R1	$-0.728\,4991$	-9.840×10^{-4}	5.2636	53.5	-1.36
	R2	$-0.728\,2116$	-9.279×10^{-4}	5.2714	50.5	1.07
	R3	$-0.702\,0525$	-7.629×10^{-4}	5.9832	41.5	-1.11
	R4	$-0.693\,5213$	-3.384×10^{-4}	6.2153	18.4	5.12
	R5	$-0.601\,5760$	-1.381×10^{-4}	8.7172	7.51	-3.68
	R6	$-0.595\,7538$	-9.317×10^{-4}	8.8756	50.7	-0.532
	R7	$-0.586\,8649$	-7.987×10^{-4}	9.1174	43.5	-0.410
$^4S^o$	R1	$-0.599\,8844$	-3.681×10^{-4}	8.7679	20.0	0.30
	R2	$-0.565\,6915$	-4.713×10^{-4}	9.6983	25.7	-0.983

notably for the spd and sdf cases and because of memory size (we construct our CI matrix up to $\sim 10\,000$ configurations), we confine the p electrons up to $n=12$. The consequence is that some thresholds, such as ^3D, ^3P are better reproduced than $^3P^o$. Such difference may be observed mainly after the first threshold, where an energy shift is manifest in our calculation in comparison with the R-matrix
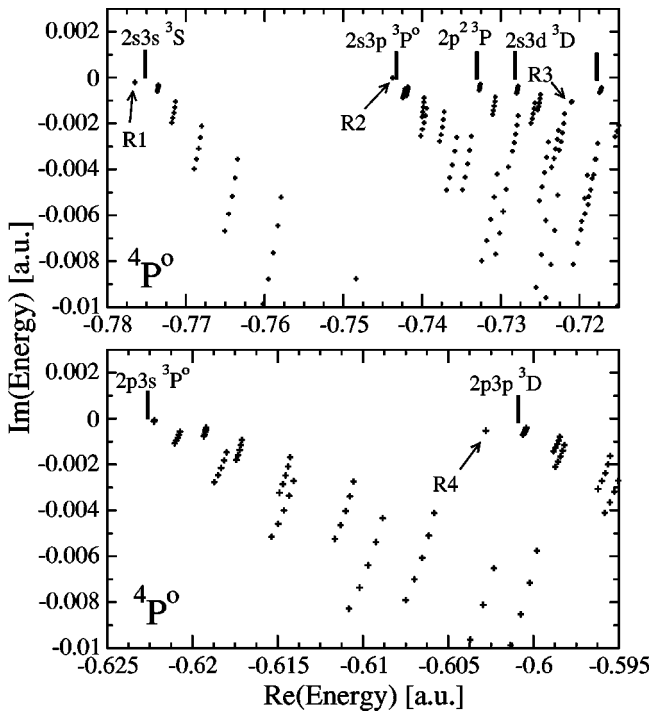
FIG. 3. Complex eigenvalue spectrum of Be$^-$ $^4P^o$ for different values of the rotation angle θ, from 8° to 16°. The eigenvalues fall into the lower half of the complex plane with an angle 2θ. The eigenvalues accumulated in fixed points—not affected by the complex rotation—show a resonance behavior and they are labeled as Rn. Vertical lines indicate the position of Be thresholds $1s^2\,nln'l'$ $^3L^\pi$.

results. Nevertheless, the threshold law tendency in our cross section is kept. The region of major interest comes after the Be($1s^2 2p^2$ ^3P) threshold. A set of resonances up to the double-ionization threshold (Be$^+$) have been found in this symmetry. The sharp peak R1 of 30.2 Mb at ~ 5.25 eV, present in other previous calculations, corresponds to a resonant state with position $E_{R1}=5.2636$ eV and width $\Gamma_{R1}=53.5$ meV, slightly above the Be($1s^2 2s3d$ ^3D) threshold position. This peak has not been regarded before as a resonance. The asymmetry of this resonance ($q=-1.36$) provokes the shift of the maximum in the cross section, to appear slightly below the Be($1s^2 2s3d$ ^3D) threshold. Our complex scaling analysis in the complex plane (see Fig. 5) allows us to identify both this R1 and the R2 eigenvalues as a S-matrix pole over the ^3D threshold. Similarly, we discover five additional small resonances in the complex plane, the last two, R6 and R7, imperceptible in the cross section. The latter are broad and slowly θ-convergent resonances, a similar case to that appearing also in the He$^-$ complex spectra [9]. Table III contains a summary of these resonances and their parameters. The cross section by Xi and Froese Fischer [18] shows a discrepancy in the threshold law but it is closer to our result in the nonresonant maximum. Surprisingly, their velocity gauge result (Fig. 5 in Ref. [18]) compares better with the length gauge R-matrix results by Ramsbottom and Bell [17] and Zeng *et al.* [19]. The discrepancy in the background above 5 eV may be attributed to the fact that we include implicitly all the contributing channels opened through the whole Rydberg series.

The photodetachment cross section for the final $^4S^o$ state in Fig. 6 has not been reported so far. The $^4S^o$ channels open at the Be($1s^2 2p^2$ ^3P) threshold at ~ 5 eV (the peak due to the metastable $2p^3$ $^4S^o$ state is omitted) and the main features contributing to the total cross section come from photon energies higher than 8 eV, i.e., from triply excited states of Be$^-$. We find two resonant triply excited states of this symmetry; R1 is a window resonance located at $E_{R1}=8.7679$ eV and width $\Gamma_{R1}=20.0$ meV and R2 is located at
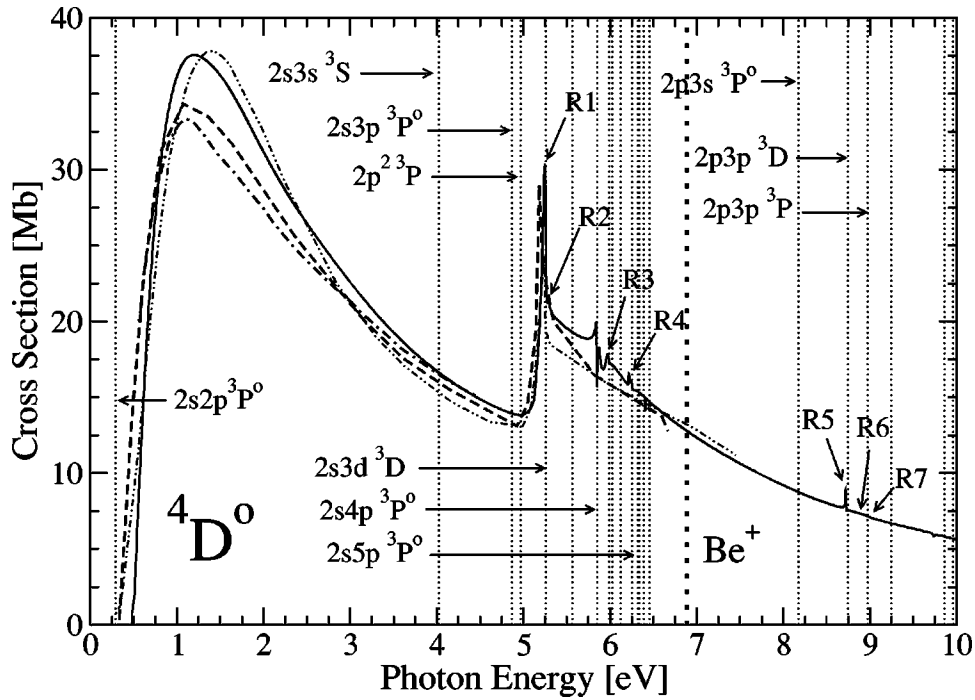
FIG. 4. Calculated photodetachment cross section to Be⁻ $^4D^o$ from the metastable Be⁻ $1s^2 2s2p^2$ $^4P^e$ state. Solid line, this work, dashed line; R-matrix by Zeng *et al.* [19], dash-dotted line, R-matrix by Ramsbottom and Bell [17], and dash-double-dotted line, Xi and Froese Fischer [18]. The rest of the notation as in Fig. 2.
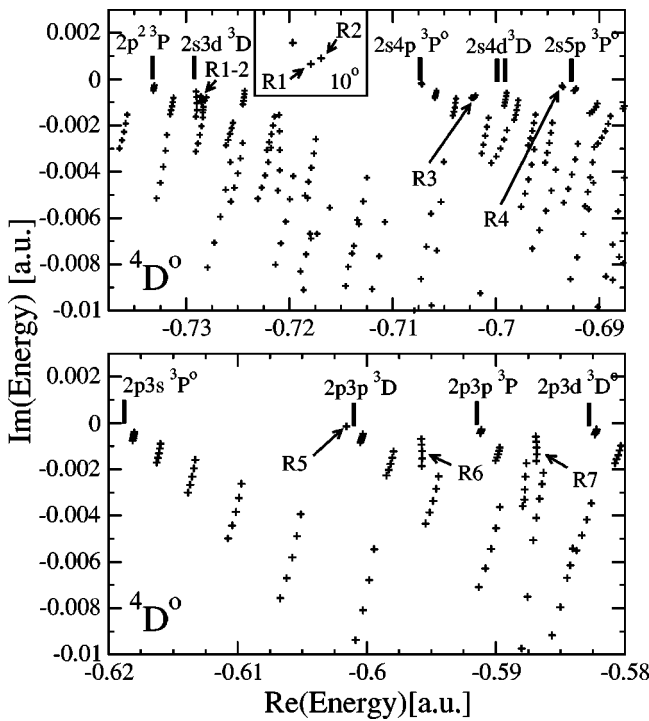
FIG. 5. Same as Fig. 3 but for the Be⁻ $^4D^o$ complex eigenvalue spectrum. The inset shows a blow up of the eigenvalues (for a fixed rotation angle) corresponding to R1 and R2 resonances, just above the eigenvalue that represents the Be $1s^2 2s3d$ ^3D threshold.

$E_{R2} = 9.6983$ eV with a width of $\Gamma_{R2} = 25.7$ meV. Both resonances are clearly identified in the complex plane in Fig. 7. Two extra small peaks above R2 are noticeable and they mimic small resonances in the cross section. Tentatively, they may be resonances but since they exactly overlap the Be($1s^2 2p4p$ ^3P) and the Be($1s^2 2p4d$ $^3D^o$) thresholds, respectively (see Fig. 7), it is difficult for us to produce a definitive answer within the complex scaling approach.
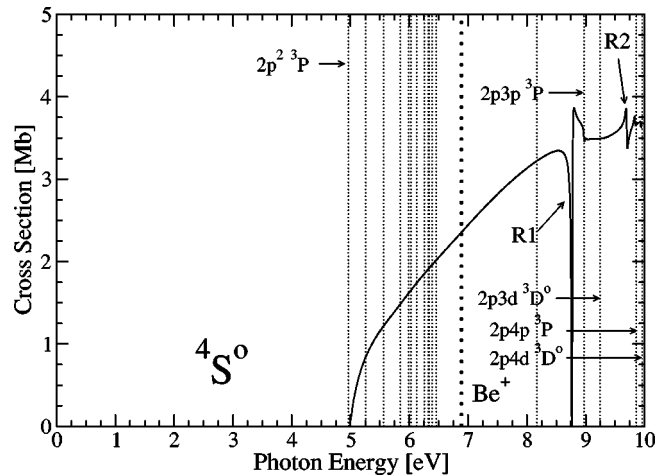
FIG. 6. Calculated photodetachment cross section to Be⁻ $^4S^o$ from the metastable Be⁻ $1s^2 2s2p^2$ $^4P^e$ state. Solid line; this work. The rest of the notation as in Fig. 2.
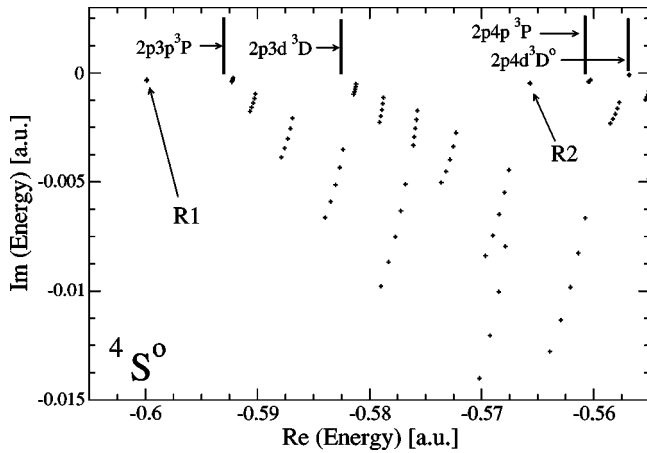
FIG. 7. Same as Fig. 3 but for the Be$^-$ $^4S^o$ complex eigenvalue spectrum.

Finally, the total photodetachment cross section is shown in Fig. 8. The major discrepancy compared to previous calculations appears just after the first Be threshold. Our result shows a shoulder coming from the $^4P^o$ symmetry, but in the R-matrix result of Zeng *et al.* [19] it is not present and we have no explanation for this. The R-matrix results by Ramsbottom and Bell [17] and the inverse-iterative Galerkin method of Xi and Froese Fischer do not provide results close enough to this threshold to compare. The two main resonances from the $^4P^o$ are in qualitative agreement with those obtained earlier by Zeng *et al.* with the R-matrix method, with a small difference in the position but considerable in strength. The resonant peak after 5 eV coming from the $^4D^o$

symmetry is reproduced by all three theories, but going further up in energy our calculation shows a much more rich structure through the Rydberg series and the extra contribution from the $^4S^o$ at ~ 8.76 eV. We think that our CSCI calculation is the most sophisticated so far, quite accurate and trustworthy, as shown in previous calculations on He$^-$, where a comparison between our CSCI results and high-resolution experimental data is very good [34]. We also include in the figure the experimental points obtained by Bae and Peterson [5] and Pegg *et al.* [15]. We will not discuss here these experiments carried out on Be$^-$ (a brief analysis is done in Ref. [17]) and their comparison with theory. It is clear that the information they provide is contradictory and insufficient to test the calculations.

IV. CONCLUSIONS

In conclusion, outer-shell photodetachment of the metastable Be $^-1s^22s2p^2$ $^4P^e$ negative ion has been calculated through a complex scaled configurations interaction method. All the final symmetries show resonant features: we find in this work four $^4P^o$ resonances, seven $^4D^o$ resonances, and two $^4S^o$ resonances. Of them, six correspond to resonant triply excited states of Be$^-$. We report parameters that characterize all these resonances. We find a basic agreement with previous theoretical results, R-matrix as well as inverse-iterative Galerkin method and we confirm the presence of two major $^4P^o$ resonances as reported before by Zen *et al.* However, the minor differences can be used to test the ability of different methods to achieve accurate results. These discrepancies appear (1) slightly in the position of the two
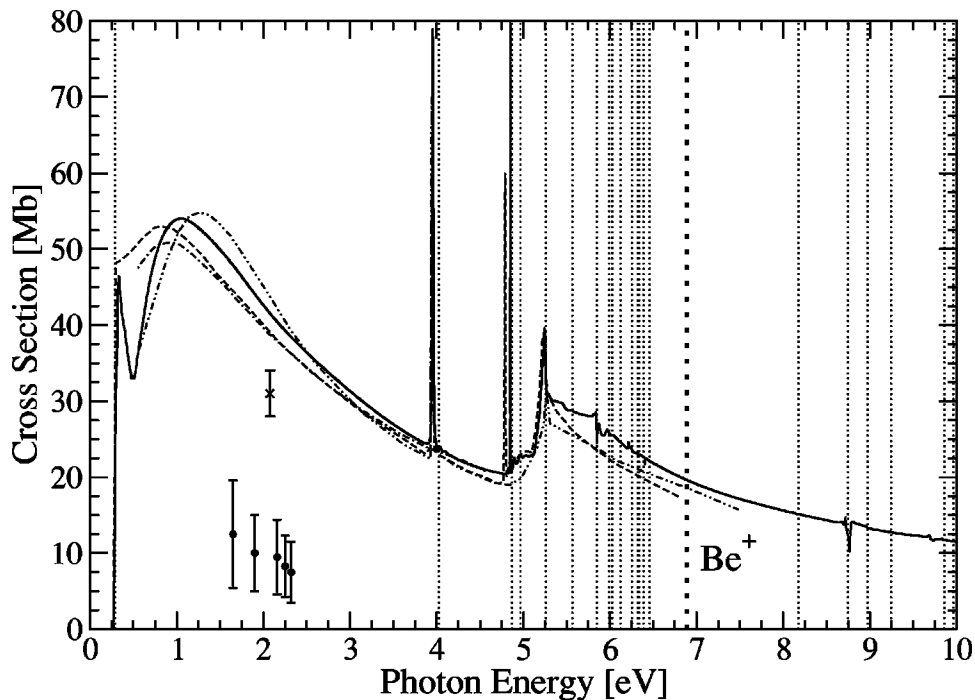
FIG. 8. Total photodetachment cross section from the metastable Be$^-$ $1s^22s2p^2$ $^4P^e$ state. Same notation as Fig. 2. Solid line, this work, dashed line, R-matrix by Zeng *et al.* [19], dash-dotted line, R-matrix by Ramsbottom and Bell [17], dash-double-dotted line, Xi and Froese Fischer [18], circles, experiment by Bae and Peterson [5], cross, and experiment by Pegg *et al.* [15].

aforementioned $^4P^o$ resonances, (2) the behavior of the cross section close to the first Be threshold, and (3) the cross section around 5 eV and beyond. Therefore, we encourage experimentalist to perform new high-resolution experiments on Be$^-$ photodetachment that can shed light on both the experimental and theoretical discrepancies.

[1] S.J. Buckman and C.W. Clark, Rev. Mod. Phys. **66**, 539 (1994).

[2] A. Hibbert, Adv. At. Mol. Phys. **18**, 309 (1982).

[3] C. Laughlin and G.A. Victor, Adv. At. Mol. Phys. **25**, 163 (1990).

[4] K. Bethge, E. Heinicke, and H. Baumann, Phys. Lett. **23**, 542 (1966).

[5] Y.K. Bae and J.R. Peterson, Phys. Rev. A **30**, 2145 (1984).

[6] A.W. Weiss, Phys. Rev. **166**, 70 (1968).

[7] L. Kim and C.H. Greene, J. Phys. B **22**, L175 (1989).

[8] J.L. Sanz-Vicario and E. Lindroth, Phys. Rev. A **65**, 060703(R) (2002).

[9] J.L. Sanz-Vicario, E. Lindroth, and N. Brandefelt, Phys. Rev. A **66**, 052713 (2002).

[10] J.F. McNutt and C.W. McCurdy, Phys. Rev. A **27**, 132 (1983).

[11] D. Frye and L. Armstrong, Jr., Phys. Rev. A **34**, 1682 (1986).

[12] M. Bentley, Phys. Rev. A **42**, 1192 (1990).

[13] D.R. Beck, C.A. Nicolaides, and G. Aspromallis, Phys. Rev. A **24**, 3252 (1981).

[14] P. Balling *et al.*, Phys. Rev. Lett. **69**, 1042 (1992).

[15] D.J. Pegg, C.Y. Tang, J.R. Wood, J. Dellwo, and G.D. Alton, Phys. Rev. A **50**, 3861 (1994).

[16] C. Sinanis, Y. Komninos, and C.A. Nicolaides, Phys. Rev. A **51**, R2672 (1995).

[17] C.A. Ramsbottom and K.L. Bell, J. Phys. B **29**, 3009 (1996).

[18] J. Xi and C.F. Fischer, J. Phys. B **32**, 387 (1999).

[19] J. Zeng, J. Yuan, and Q. Lu, Phys. Rev. A **62**, 022713 (2000).

[20] H. Bachau, P. Galan, and F. Martin, Phys. Rev. A **41**, 3534 (1990).

[21] M. Aymar, G.H. Greene, and E. Luc-Koenig, Rev. Mod. Phys. **68**, 1015 (1996).

[22] C.H. Maier, L.S. Cederbaum, and W. Domcke, J. Phys. B **13**, L119 (1980).

[23] T.N. Rescigno and V. McKoy, Phys. Rev. A **12**, 522 (1975).

[24] S. Bashkin and J. O. Stoner, *Atomic Energy Levels and Gotrian Diagrams* (North-Holland, Amsterdam, 1975).

[25] E. Lindroth, Phys. Rev. A **52**, 2737 (1995).

[26] D.W. Norcross and M. Seaton, J. Phys. B **9**, 2983 (1976).

[27] J. Olsen, L.G.M. Pettersson, and D. Sundholm, J. Phys. B **37**, 5575 (1994).

[28] C. Pan, A.F. Starace, and C.H. Greene, Phys. Rev. A **53**, 840 (1996).

[29] G. Haeffler, I.Y. Kiyan, U. Berzinsh, D. Hanstorp, N. Brandefelt, E. Lindroth, and D.J. Pegg, Phys. Rev. A **63**, 053409 (2001).

[30] NIST Atomic Spectra DataBase, web page: http://physics.nist.gov

[31] J-J. Hsu and K.T. Chung, Phys. Rev. A **52**, R898 (1995).

[32] C.L. Peckeris, Phys. Rev. **112**, 1649 (1958).

[33] P. Kristensen, V.V. Petrunin, H.H. Andersen, and T. Andersen, Phys. Rev. A **52**, R2508 (1995).

[34] R. C. Bilodeau and N. Berrah (private communication).